PPPL 1854
UC20 F

MASTER

Analysis of Mirnov Oscillations on PDX

By

G. Hammett and K. McGuire

February 1982

PLASMA PHYSICS LABORATORY

PRINCETON UNIVERSITY
PRINCETON, NEW JERSEY

PREPARED FOR THE U.S. DEPARTMENT OF ENERGY,
UNDER CONTRACT DE-AC02-76-CHO-3073.

Analysis of Mirnov Oscillations on PDX*

PPPL--1854

DE82 009816

G. Hammett and K. McGuire

Princeton University, Plasma Physics Laboratory

Princeton, New Jersey 08544

Abstract

Mirnov coils have been used to study MHD oscillations in PDX. We first review the information that can be obtained from Mirnov coils concerning the amplitude of these oscillations and their toroidal and poloidal mode numbers. The usual techniques for analyzing Mirnov coil data do not work well on PDX because of the rectangular arrangement of the coils, substantial noise levels, and poloidal amplitude asymmetries. A technique using digital Fourier analysis to focus attention on the fundamental frequency component of the signals has been successful in determining the m and n mode numbers of Mirnov oscillations in the PDX tokamak.

---

*Work supported by the U.S. Department of Energy, Contract No DE-AC02-76-CHO-3073.

I. Introduction

A detailed understanding of MHD activity in a tokamak plasma is needed in order to control major disruptions and obtain low q discharges. The control of major disruptions is of utmost importance for the future of large tokamak devices. Magnetic islands play a prominent role in the theory of disruptions. Their structure is approximately of the form $e^{i(m\theta + n\phi)}$, where θ is the poloidal angle and ϕ is the toroidal angle, and they are located radially on the $q = m/n$ surface.

Mirnov first used B_θ loops to study MHD oscillations [1]. Mirnov coils are simple loops of wire used to measure local magnetic fields. A typical arrangement is shown in Fig. 1. They are mounted outside the plasma at various poloidal and toroidal angles. Figure 2(a) shows a typical measurement of the Mirnov coils at a single instant in time. The B-field perturbation is plotted as a function of θ.

One might assume that this field perturbation was caused by an m=3 magnetic island. But the Mirnov coils are outside the plasma and do not measure the field strength on the $q = 3/n$ surface. Other than counting the number of maxima in the field strength plot, it is not obvious what one can say about internal current distribution based on external field measurements. Section II derives a well-known relation between the Fourier transform of the external field and the moments of the internal current distribution in cylindrical geometry. First order toroidal corrections to the simple cylindrical model are then discussed.

Standard techniques of analyzing Mirnov oscillations face several problems on PDX (the Poloidal Divertor Experiment). First, the PDX tokamak has a rectangular vacuum vessel, so the Mirnov coils are not mounted in a circle. Second, the Mirnov coils are only located on the inside and outside

walls (Fig. 3). We plan to add more coils above and below the plasma in the future. Third, the Mirnov coils pickup a significant amount of noise. Much of the noise is at multiples of 720 Hz and comes from the PDX power supplies. Finally, there is frequently a large poloidal asymmetry in the amplitude of Mirnov oscillations. Section III outlines a Fourier technique which determines the m and n mode numbers of the oscillations by fitting the phase shifts between different Mirnov coils. This technique has successfully overcome the problems listed above. Section III concludes with an example of Mirnov oscillations in PDX.

II. Moments of the Current Distribution

If a current in the $\hat{z}$ direction is distributed over a circle with density proportional to $\cos(m\theta-\theta_o)$, then the resulting poloidal B_θ field also varies as $\cos(m\theta - \theta_o)$; A proof of this is presented here. This is a well known result and the present discussion in a cylindrical geometry is based on a paper by Righetti [2]. To zeroth order in the aspect ratio, we can consider the cylindrical geometry of Fig. 2(a). A single, infinitely long line carrying a current I out of the page is located at (r,θ_o). If $r = 0$, the $\vec{B}$ field is (SI units are used throughout):

$$\vec{B} = \frac{\mu_o I}{2\pi a}\,\hat{\theta}\ .$$

For $r \neq 0$, $\vec{B}$ is written more generally as:

$$B_\theta = \frac{\mu_o I}{2\pi}\cdot\frac{a - r\cos(\theta - \theta_o)}{a^2 + r^2 - 2ar\cos(\theta - \theta_o)} \qquad (1)$$

$$B_r = -\frac{\mu_o I}{2\pi} \frac{r \sin(\theta - \theta_o)}{a^2 + r^2 - 2ar\cos(\theta - \theta_o)} . \qquad (2)$$

The denominator can be factored into $[a-re^{i(\theta - \theta_o)}]\ [a-re^{-i(\theta - \theta_o)}]$. Using the method of partial fractions, we can expand B_θ into:

$$B_\theta = \frac{\mu_o I}{2\pi} \frac{1}{2} \left[\frac{1}{a-re^{i(\theta - \theta_o)}} + \frac{1}{a-re^{-i(\theta-\theta_o)}}\right] .$$

We can expand this in powers of r/a or a/r, depending on whether the line current I is inside or outside the circle. Following these same steps for B_r, we get:

$\underline{r < a}$

$$B_\theta = \frac{\mu_o I}{2\pi a} \sum_{n=0}^{\infty} \left(\frac{r}{a}\right)^n \cos n(\theta - \theta_o)$$

$$B_r = -\frac{\mu_o I}{2\pi a} \sum_{n=0}^{\infty} \left(\frac{r}{a}\right)^n \sin n(\theta - \theta_o)$$

$\underline{r > a}$

$$B_\theta = -\frac{\mu_o I}{2\pi a} \sum_{n=1}^{\infty} \left(\frac{a}{r}\right)^n \cos n(\theta-\theta_o)$$

$$B_r = -\frac{\mu_o I}{2\pi a} \sum_{n=1}^{\infty} \left(\frac{a}{r}\right)^n \sin n(\theta - \theta_o) .$$

We have now expanded $\vec{B}$ as a Fourier series, and each coefficient is simply related to the position r,θ_o of the current I. In fact, the proper sum of fourier coefficients allows us to look only at the current inside the cylinder, while ignoring any current outside the cylinder. Using the orthogonality of fourier series we get:

$$a\int_0^{2\pi} B_\theta(\theta)\cos m\theta\, d\theta - a\int_0^{2\pi} B_r(\theta)\sin m\theta\, d\theta = \begin{cases} \mu_o I \left(\frac{r}{a}\right)^m \cos m\theta. & \text{If } r < a \\ 0 & \text{If } r > a \end{cases} \tag{3}$$

$$a\int_0^{2\pi} B_\theta(\theta)\sin m\theta\, d\theta + a\int_0^{2\pi} B_r(\theta)\cos m\theta\, d\theta = \begin{cases} \mu_o I \left(\frac{r}{a}\right)^m \sin m\theta_o & \text{if } r < a \\ 0 & \text{if } r > a \end{cases} . \tag{4}$$

The straightforward way of proving Eqs. (3) and (4) is to substitute for B_θ and B_r using Eqs. (1) and (2). The integrals could then be evaluated as contour integrals in the complex plane. However, it is much easier to use the trick of expanding B_θ and B_r in Fourier series and use their orthogonality property.

If the Mirnov coils are mounted just inside a conducting shell, then $B_r = 0$ and the second terms in Eqs. (3) and (4) vanish. Instead of a single line current I at (r,θ_o), consider a general toroidal current density $j(r,\theta)$. $\vec{B}$ is just a linear superposition of the B-fields produced by each of the infinitesimal line currents $j(r,\theta)\, r dr d\theta$. We must replace the right hand side of the Eqs. (3) and (4) with an integral over the current distribution. Using complex notation this yields:

$$a\int_0^{2\pi} B_\theta(\theta)\, e^{im\theta}\, d\theta = \mu_o \int_0^a dr \left(\frac{r}{a}\right)^m \int_0^{2\pi} r d\theta\, j(r,\theta) e^{im\theta} \quad . \tag{5}$$

This relates the moments of the external $\vec{B}$ field with the moments of the internal current density. Continuous sin $m\theta$ and cos $m\theta$ coils have been used by many researchers to measure the integral on the left hand side of Eq. (5) for a few small values of m [3]. The coil winding density (number of turns per cm) varies as sin $m\theta$ or cos $m\theta$ (Fig. 2c). In particular, for m=0, we have a Rogowski coil which measures the total current. For m=1, we measure the average x and y position of the current distribution:

$$a\int_{o}^{2\pi} B_{\theta}(\theta)e^{i\theta}\, d\theta = \frac{\mu_o}{a}\iint_{r<a} dxdy\; j(x,y)\;(x + iy) \quad .$$

At this point we can recognize the fundamental difficulty of analyzing Mirnov oscillations. Without more assumptions, it is not possible to work backwards from the measured external $\tilde{B}$ field to find the internal current distribution. This is because the left hand side is an integral over θ only, while the right hand side integrates over r and θ.

The usual assumption is to expand the current distribution in normal modes. The cylindrical (infinite aspect ratio) normal modes are:

$$j(r,\theta) = j_o(r) + \sum_{m,n} j_{mn}\, e^{i(m\theta + n\,\phi - \omega_{mn}t)}\, \delta(r - r_{mn}) \qquad (6)$$

where $j_o(r)$ = equilibrium current distribution,

j_{mn} = amplitude of current perturbation localized at the radius r_{mn},

r_{mn} = radius of the $q = m/n$ surface,

$\delta(r - r_{mn})$ = delta function which limits the current perturbation to the rational q surface ($q = m/n$).

θ = poloidal angle,

ϕ = toroidal angle,

ω_{mn} = frequency of the m,n mode.

The fluctuating poloidal B field, $\tilde{B}_\theta$, produced by the j_{mn} current perturbation is simply:

$$\tilde{B}_\theta(r,\theta,\phi) = \mu_o j_{mn} r_{mn} \left(\frac{r_{mn}}{r}\right)^{m+1} e^{i(m\theta + n\phi - \omega_{mn}t)} \quad (\text{for } r > r_{mn}).$$

We have changed notation here and in following equations: r is the radius where B_θ is measured; r_{mn} is the radius of the current perturbation. r and θ are defined with respect to the center of the resonant surface $q = m/n$. This is the fundamental equation used to analyze Mirnov oscillations. There are corrrections to this equation for a finite aspect ratio tokamak which will be discussed later. But the essential method is illustrated with this simple cylindrical model.

Before moving to the toroidal corrections to the simple cylinder, we will write the equation for $\tilde{B}_y$ which is appropriate for the square vacuum vessel of PDX. The positions of some of the coils on PDX are shown in Fig. 3. All coils measure $\tilde{B}_y$ and are located not only at various θ and ϕ, but also at different radii (r) from the center of the plasma. Ignoring eddy currents induced in the vacuum vessel wall, a current perturbation of the form

$$j_{mn} \cos[m(\theta - \theta_o)]\ \delta(r - r_{mn})$$

where $\theta_o = (-n\phi - \omega t)/m$ represents the arbitrary phase of the perturbation, will produce the field

$$\tilde{B}_\theta = \frac{\mu_o j_{mn} r_{mn}}{2} \left(\frac{r_{mn}}{r}\right)^{m+1} \cos m(\theta - \theta_o) \qquad (\text{for } r > r_{mn})$$

$$\tilde{B}_r = -\frac{\mu_o j_{mn} r_{mn}}{2} \left(\frac{r_{mn}}{r}\right)^{m+1} \sin m(\theta - \theta_o)$$

$\tilde{B}_y$ is found by simply adding components and using a trigonometric identity:

$$\tilde{B}_y = \tilde{B}_\theta \cos\theta - \tilde{B}_r \sin\theta = \mu_o j_{mn} \left(\frac{r_{mn}}{r}\right)^{m+1} \cos\left[m\theta + \theta - m\theta_o\right] \qquad (\text{for } r > r_{mn}). \tag{8}$$

Note that the phase of $\tilde{B}_y$ varies as $(m+1)\theta$ while the phase of $\tilde{B}_\theta$ varies like $m\theta$.

While a cylindrical model is adequate for a qualitative understanding of Mirnov oscillations, a more realistic model of a tokamak is sometimes useful for analyzing experimental data. The field perturbations $\tilde{B}_{mn}$ due to the j_{mn} mode are different from a cylinder because of three toroidal effects

(Fig. 4). First, the perturbation j_{mn} will produce a stronger field on the inside of the torus than on the outside because the transformation which maps a cylinder into a torus does not conserve area and $\nabla \cdot B = 0$. Second, the perturbation is no longer centered on R_o, but is shifted outward by the Grad-Shafranov shift, $\Delta_p(r)$. This places the mode closer to the outside Mirnov coils. Finally, the compression of flux surfaces on the outside makes the pitch of the field larger there, so that the mode no longer has a simple $\cos m\theta$ dependence. Fussman [4] has derived an analytic expression for the B-field of current perturbations in a torus. To first order in inverse aspect ratio:

$$\tilde{B}_\theta = \frac{\mu_o j_{mn} r_{mn}}{2} \left(\frac{r_{mn}}{r}\right)^{m+1} \cos[m\theta^* + n\phi - \omega t] \qquad (\text{for } r > r_{mn}). \tag{9}$$

where $\theta^* = \theta - \lambda \sin\theta$,

$\lambda = r_{mn}/R_o \, (1 + \ell_i/2 + \beta_\theta)$,

ℓ_i = internal inductance, at the resonant flux surface of radius r_{mn}

β_θ = poloidal beta at the resonant flux surface

r = distance from center of resonant surface at $R_o + \Delta_p(r_{mn})$ to the Mirnov coil at (r,θ,ϕ).

R_o = major radius of plasma

The formula for $\tilde{B}_y$ is exactly the same except that $m\theta^*$ is replaced by $(m\theta^* + \theta)$. A similar formula is derived by Merezhkin [5] and compared with

experimental measurements on the T-6 tokamak. He found that the transformation $\theta \rightarrow \theta^*$ fits the measured phase data fairly well. He also measures a poloidal asymmetry $B_\theta(\theta=0)/B_\theta(\theta=\pi)$ which ranges from .7 to 1.8 but he does not discuss possible causes of this asymmetry.

Potentially significant errors may develop if one analyzes real Mirnov oscillations from a tokamak with the cylindrical model (Eq. 7) instead of the toroidal model (Eq. 9). deKock [3] has discussed the magnitude of these errors. For example, if a single m = 2, n = 1 current perturbation existed at the q = 2 surface, the resulting $\tilde{B}_\theta$ field would appear to have components of other m, n values also, unless the λ and Δ_p corrections are properly included. Figure 5 shows how the transformation $\theta \rightarrow \theta^*$ corrects this situation.

III. A Fourier Transform Method for Analyzing Mirnov Oscillations

Ideally, Mirnov coils should tell us the amplitudes, phases, and rotation frequencies of all modes present in the plasma as a function of time. For a large aspect ratio tokamak with low β this can easily be done with the cylindrical model of the last section. With a set of Mirnov coils spanning a poloidal cross-section, one takes the Fourier transform in θ to yield the amplitudies of each component $\cos(m[\theta - \theta_o])$ as a function of time. An ingenious technique for doing this by analog multipexing has been developed and used on many tokamaks [6].

The Fourier-transform-in-θ technique has not been feasible on PDX for many reasons. The rectangular geometry of the vacuum vessel and the use of poloidal divertors prevented the usual placement of Mirnov coils to measure $\tilde{B}_\theta$ as a function of θ which is needed to estimate B_θ's Fourier transform

in θ. 720 Hertz ripple in the ohmic and equilibrium fields show up as noise on the Mirnov coils. An amplitude asymmetry which is not yet understood would make a naive attempt at Fourier transforming in θ prone to significant errors. On PDX, the ratio of perturbation amplitudes at $\theta = 0$ and $\theta = \pi$, $\tilde{B}_{out}/\tilde{B}_{in}$, varies from .5 to 6, and is typically around 3. To illustrate the type of analysis error this produces, assume that the amplitude asymmetry in $\tilde{B}_\theta$ can be parameterized by:

$$\tilde{B}_\theta = B_1 \, (1 + \gamma \cos\theta) \cos(m\theta - \omega t) \, .$$

Where $(1 + \gamma)/(1-\gamma)$ is the size of the asymmetry $\tilde{B}_{out}/\tilde{B}_{in}$. Using a trig identity this can be rewritten as:

$$\tilde{B}_\theta = B_1\left[\cos(m\theta - \omega t) + \frac{\gamma}{2}\cos((m-1)\theta - \omega t) + \frac{\gamma}{2}\cos\left((m+1)\theta - \omega t\right)\right] .$$

The transform-in-θ technique would interpret this as three different modes (m, m+1, m-1) which just happen to be rotating at exactly the same frequency. The transform-in-time technique to be discussed next would interpret this as a single mode because the phase varies only as $m\theta$. We prefer this interpretation, which ignores the amplitude asymmetry, because the asymmetry seems to be much larger than predicted by the Grad-Shafranov shift and other toroidal corrections.

It is easy to make erroneous conclusions if the subtlety of the situation is not appreciated. The moments of B_θ yield the moments of j_z. To say that a single mode is measured means that a current perturbation of the approximate form $\cos(m\theta + n\phi - \omega t)$ on the $q = m/n$ surface exists. This does not imply that the only magnetic islands are on the $q = m/n$ surface. Toroidal

eigenmodes and cylindrical eigenmodes do not have exactly the same form, although each toroidal eigenmode can can be identified as a perturbed cylindrical eigenmode. In particular, Fussman [4] has shown that in a toroidal tokamak geometry, a current perturbation on the q = m/n surface generates islands not only at the q = m/n surface, but also generates other islands of different helicities at other flux surfaces, although these islands are smaller.

In order to deal with these problems, we have developed a technique based on taking the Fourier transform in of each Mirnov signal during a selected time window. The relationship between the phases of different Mirnov signals identifies m and n without looking at the amplitudes of the signals. By looking at the signals in the frequency domain we are able to reject noise and other modes at frequencies other than ω_{mn} and we are able to accurately measure the relative phases of signals. A similar technique has been used at Oak Ridge [7].

The best way to explain the technique is with an example. Figure 6 shows the experimental setup of Mirnov coils on PDX. Figure 7 shows the plasma current and 14 Mirnov signals as a function of time (only ~ 300 msecs of Mirnov data is digitized). The Mirnov oscillations slow down and stop altogether at 420 msecs. The signals after that represent the noise level. An expansion of 10 msecs is shown in Fig. 8. A peak appears first on coil 1 and progresses to coil 5 (see Fig. 5 for the position of these 5 coils. This mode is rotating in the electron diamagnetic direction. Coils 12 and 13 are at the same toroidal angle, but coil 12 is at $\theta=0$ while coil 13 is at $\theta=\pi$. They both measure $\tilde{B}_\theta$ (note that for coil 13, $B_\theta = - B_y$). They are in phase and we can conclude that m is an even integer. The amplitude asymmetry is $B_{12}/B_{13} \cong 2$.

The power spectrum (Fig. 9) for these 14 signals shows that the fundamental component has a frequency of 1.3 kHZ. The fundamental component of the $\tilde{B}_y$ signal measured by the i'th coil can be written as

$$S_i = A_i \cos(2\pi(1300)t - \delta_i)$$

where δ_i is the phase lag of the i'th signal.

According to the last section the predicted phase shift δ_i^* for the m,n mode is:

$$\delta_i^* = m(\theta_i - \lambda\sin\theta_i) + \theta_i + n\,\phi_i + \delta_o + k_i\,2\pi \qquad (k_i = \text{integer})$$

where (θ_i, ϕ_i) gives the location of the i'th Mirnov coil, and $\delta_o + k_i 2\pi$ expresses the multi-valued property of phase. Figure 10a plots the experimental δ_i data points and the best fit of δ_i^* through them. (Strictly speaking, the data points which are plotted are $\delta_i - n\phi_i$, so that the toroidal dependence is removed.) A line with slope 3 fits the data fairly well, so m = 2, n = 1. In generating this plot, δ_o and the k_i were chosen to make the data fit the line as well as possible.

Figure 10(b) plots the data with the best choice of δ_o and k_i for (m,n) = (2,0). The three coils at a different toroidal location obviously do not fit. Therefore n is determined to be 1 and not 0. This is made quantitative by the reduced Chi-square statistic, defined as:

$$\chi_r^2 = \frac{\sum_{i=1}^{N} (\delta_i - \delta_i^*)^2}{(N - \nu)\sigma^2}$$

where δ_i = the dependent variable,

θ_i, ϕ_i = the independent variables,

δ_i^* = the predicted phase shift $\delta_i^* = m\theta^*_i + \theta_i + n\phi_i + \delta_o + k_i 2\pi$,

ν = number of parameters in the fitting function (3),

N = number of data points (14).

σ^2 = expected variance of data (assuming uniform distribution on $[-\pi, \pi]$, $\sigma^2 = \pi^2/3$).

If the δ_i are random, then any attempt fit will yield a $\chi^2_r \sim 1$. If one particular m,n mode fits the data well then $\chi^2 \to 0$ as the fit gets better. For (m,n) = (2,1), $\chi^2_r = .017$ which is very good. The probability that this was not a random accident is greater that .9995. The (m,n) = (2,0) fit is not as good, $\chi^2_r = .440$ (Fig. 13). To see that this is significantly worse in a statistical sense, we form the F statistic F = (.440)/(.017) with 11 and 11 degrees of freedom. Looking in a table of the F-statistic distribution, we find that it is a highly improbable value. Thus it is safe to assume that the mode numbers (m,n) are (2,1) and not (2,0).

Attempted (3,1) and (4,1) fits are illustrated in Figs. 10(c) and 10(d). The (3,1) fails miserably because the real mode has even m. The (4,1) isn't quite as bad but it is still obviously wrong. The analysis program automatically checks many possible (m,n) values for possible fits and tells the program user which modes fit best.

We turn to another example to examine the robust qualities of this analysis procedure. Figure 11 shows plasma current and 16 Mirnov signals. Figure 12 is a 5 millisecond expansion of these signals. The signal-to-noise ratio is worse, while the amplitude asymmetry is less, than the signals in Fig. 8. The jagged appearance of the waveforms is because the sampling

frequency of the digitizers was 20 kHz, giving ~8 data points per cycle. Note that the mode appears to be rotating in the opposite direction from the last example. Indeed the mode numbers are identified as m=-2,n=-1 signifying rotation in the ion cyclotron direction. These oscillations occured during neutral injection which spins the plasma in the toroidal direction thus shifting the frequency of rotation. (A helical island is a bit like a barber shop pole, toroidal motion can appear to be poloidal rotation, or vice versa). The power spectrum (Fig. 13) no longer shows a nice peak at the fundamental frequency, in part because the mode was speeding up during the period 230-240 msecs. Nevertheless, the oscillations are positively identified as m=-2, n=-1 (Fig. 19). In fact, no matter which frequency the user selects from the interval 2.4 KHz to 2.8 KHz, the relative phases of that frequency component will still reveal the m=2, n=1 mode.

The toroidal correction to the phase ($\theta^* = \theta - \lambda \sin\theta$) usually gives a slightly better fit than the cylindrical model. Figure 14(a) assumed $\lambda \approx 1.6 * (20/144) = .22$. In Fig. 14(b), the toroidal correction is ignored by setting the radius of the q=2 surface to zero. The fit is still pretty good but χ^2 is 50% worse than the case where the toroidal correction is included.

The computer program which performed the above analysis is fairly straightforward. It first performs a fast Fourier transform. The program user then types in a desired frequency component to be analyzed. The phases of the signals at that frequency are fit using a non-linear grid search algorithm [8]. A non-linear fit must be used instead of a standard least-squares regression because $\theta^* = \theta - \lambda \sin\theta$ is non-linear, the squared residual $[\delta_i - f(\theta_i, \phi_i)]^2$ lies on the interval $[0,\pi^2]$, and k_i is restricted to integer values.

IV. Summary

The Fourier-transform-in-time technique has been successful on PDX in identifying the m and n mode numbers of Mirnov oscillations. It is able to accurately measure phase shifts between signals by rejecting noise at frequencies other than ω_{mn}. This also has the theoretical capability of analyzing many modes at once as long as they rotate at different frequencies. Predicted toroidal corrections to the simple $e^{i(m\theta+n\phi)}$ island structure are accurate in explaining experimental data. The transform-in-time technique utilizes phase information only. It is therefore able to ignore amplitude asymmetries, which the transform-in-θ technique can not do. However, the transform-in-θ technique is more useful in analyzing the time development of various modes.

REFERENCES

[1] S.V. Mirnov, Soviet Atomic Physics, 30, 22 (1971) (The Consultant's Bureau).

[2] G.B. Righetti, Laboratori Gas Ionizati, LGI/R/TOR.FI/73.4/E, (1973).

[3] For example, see Alcator Group, L.C.J.M. deKock et. al., M.I.T. report PRR 7414 (1974).

[4] G. Fussman, B.J. Green, H.P. Zehrfeld, Plasma Physics and Controlled Nuclear Fusion Research (Proc. Int. Conf. Brussels, 1980).

[5] V.G. Merezhkin, Sov. J. Plasma Physics, 4, 152 (1978).

[6] R.S. Granetz, M.I.T. report PFC/RR-81-25 (1981).

[7] A.P. Navarro, J.L. Dunlap, V.K. Pare, R.D. Burris, ORNL. Reprint of Poster presented at Third APS Topical Conference on High Temperature Plasma Diagnostics (1980).

[8] Phillip R. Bevington, Data Reduction and Error Analysis for the Physical Sciences, McGraw-Hill.

FIGURES

1. An example of the placement of Mirnov coils.

2. (a) Hypothetical picture of $\tilde{B}_\theta$, the fluctuating part of B_θ, as a function of θ at a single instant in time.

   (b) Cylindrical geometry of Eqs. (1) - (4).

   (c) "cos θ" coil which measures the average x position of the plasma current.

3. Positions of some of the Mirnov coils in PDX. The vacuum vessel is the racetrack shape which encircles the Mirnov coils. The flux surfaces are denoted by nested dotted lines in the plasma region and by solid lines in the scrapeoff region.

4. Toroidal distortions of the cylindrical model:

   (a) Bending a straight wire into a loop creates a stronger magnetic field inside the loop than outside the loop.

   (b) The Grad-Shafranov shift, $\Delta p(r)$, moves the perturbation outward.

   (c) Distortion of $\cos(m\theta)$ dependence of the island caused by greater field line pitch at the outside ($\theta = 0$) edge of the torus.

5. Toroidal correction to the phase. The top graph shows $B_\theta(\theta)$ in a tokamak with a/R = .3, $l_i 2 + B_\theta = 1$, and an m=2 current perturbation. Mapping $\theta \to \theta^*$ in the second graph reveals the cos(2θ) current perturbation, while the first graph mistakenly identifies m=1 and m=3 components existing in addition to the dominant m=2 contribution.

6. Experimental setup of Mirnov coils in PDX.

7. Mirnov signals measured at 14 positions in PDX. (Circular Plasma, R = 143 cm, a = 44 cm).

8. Expansion of the time axis of Fig. 7.

9. Power spectrum for the signals for Fig. 8. Power is $\left|\dot{\tilde{B}}_\theta\right|^2$ in arbitrary units on a linear scale.

10. Phase plots to determine m and n, for Fig. 8. Phase of the 1.3 kHz component of each signal is plotted versus the poloidal angle θ where the signal $\dot{\tilde{B}}_y$ was measured.

    (a) m=2, n=1, χ_r = 0.17, probability of being a non random fit > .995.

    (b) m=2, n=0, χ_r = .440, probability of being a non random fit = .938.

    (c) m=3, n=1, χ_r = 1.106, probability = .351.

    (d) m=4, n=1, χ_r = .249, probability = .994.

11. Mirnov signals measured at 16 positions in PDX. (Discharge parameters: square plasma, R= 143 cm, a = 42 cm.)

12. Expansion of the time axis of Fig. 11.

13. Power spectrum $(\dot{B}_\theta^2)$ for the signals of Fig. 12.

14. Phase plots to determine m and n, for Fig. 12. Phase of the 2.6 kHz component of each signal is plotted versus the poloidal angle where the signal ($\dot{B}_y$) was measured.

    (a) m=-2, n=-1, χ_r = .020, probability > .9995. Model parameters: R = 144 cm, r_{mn} = 20 cm, $l_i/2 + B_\theta$ = .6.

    (b) M=-2, n=-1, χ_r = .031, probability > .995. Model parameters: R = 144 cm, r_{mn} = 0, $l_i/2 + B_\theta$ = 0.

#81X1410

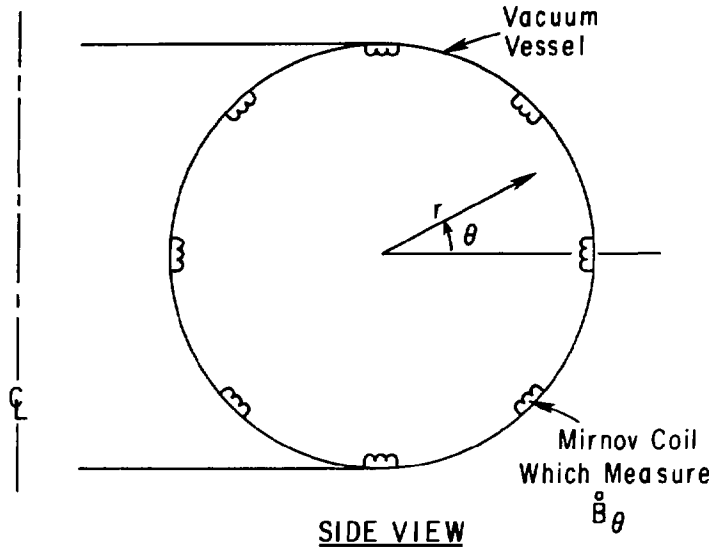

SIDE VIEW

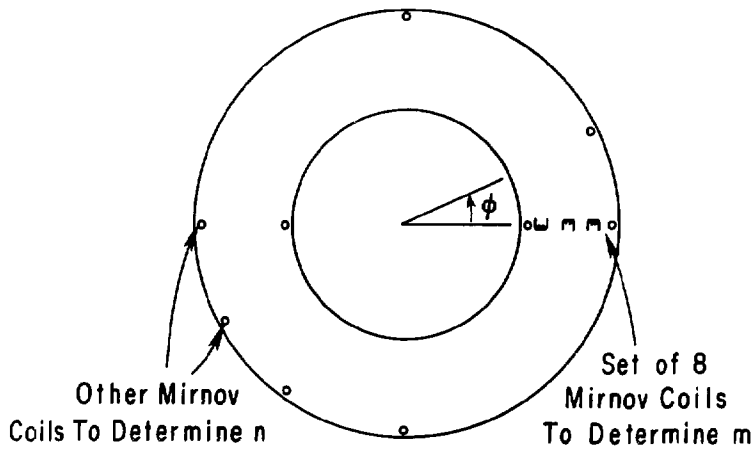

TOP VIEW

Fig. 1

#81X1408

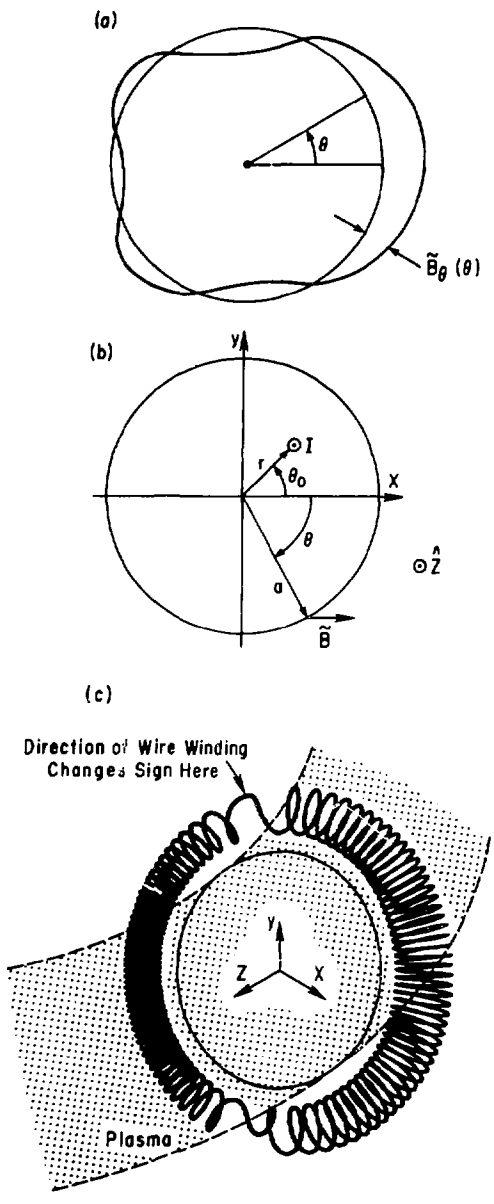

Fig. 2

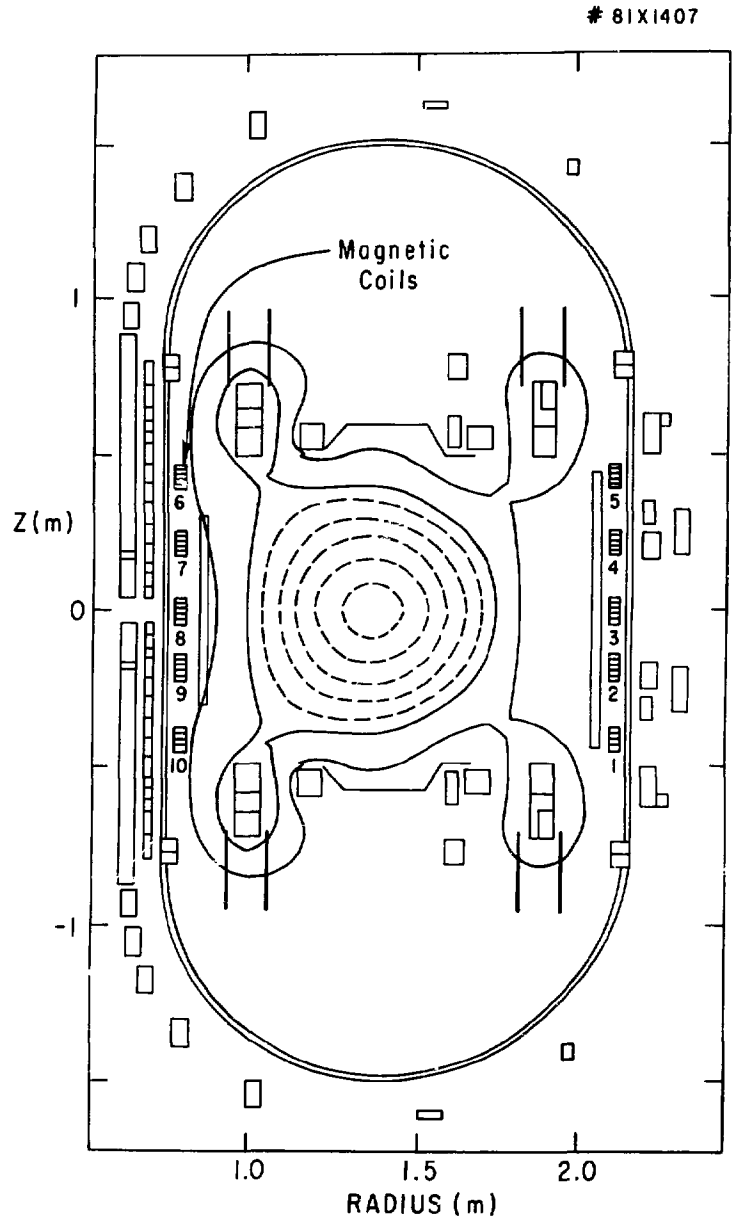

Fig. 3

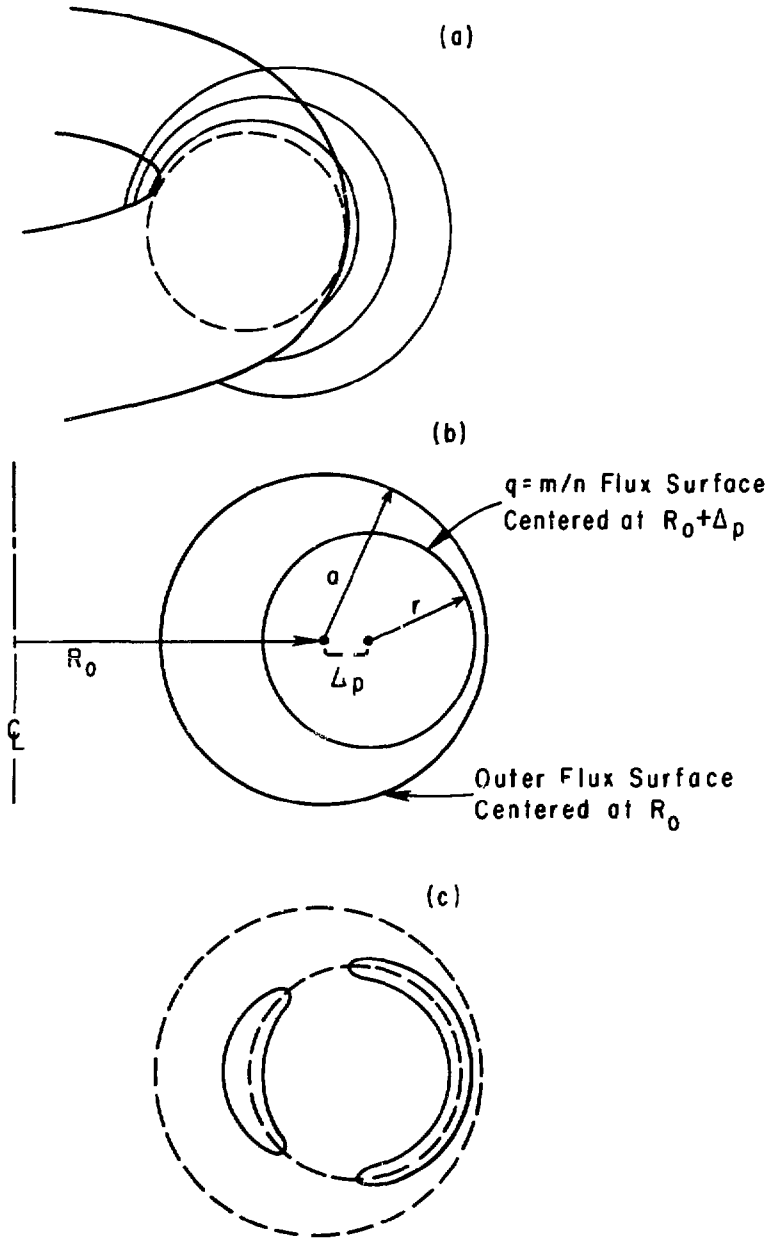
(a)
(b)
q = m/n Flux Surface
Centered at $R_0+\Delta_p$
a
r
R_0
Δ_p
Outer Flux Surface
Centered at R_0
(c)

Fig. 4

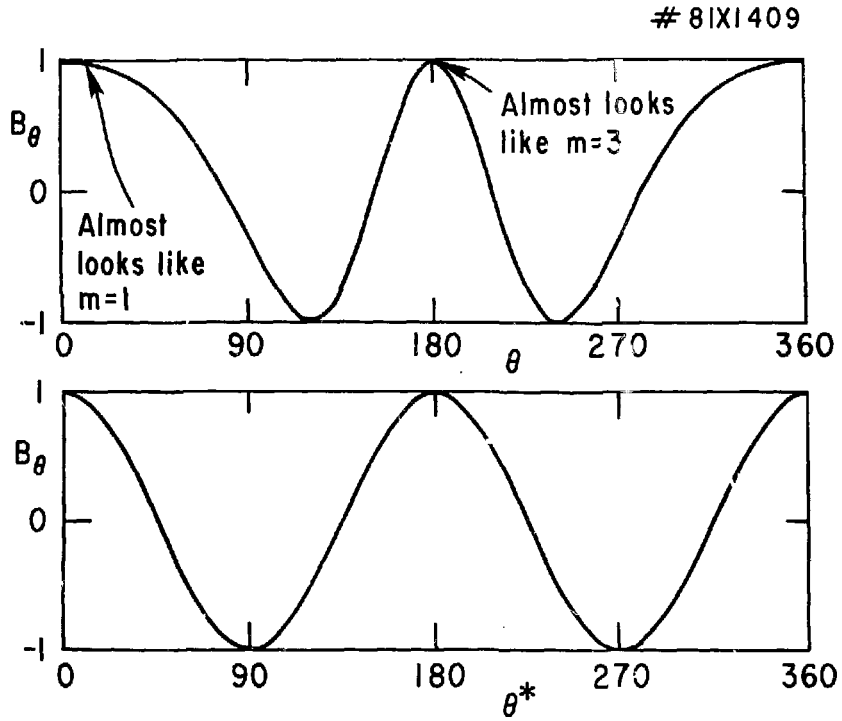
#81X1409
1
B_θ
0
-1
Almost looks like m=1
Almost looks like m=3
0
90
180
270
360
θ
1
B_θ
0
-1
0
90
180
270
360
θ^*

Fig. 5

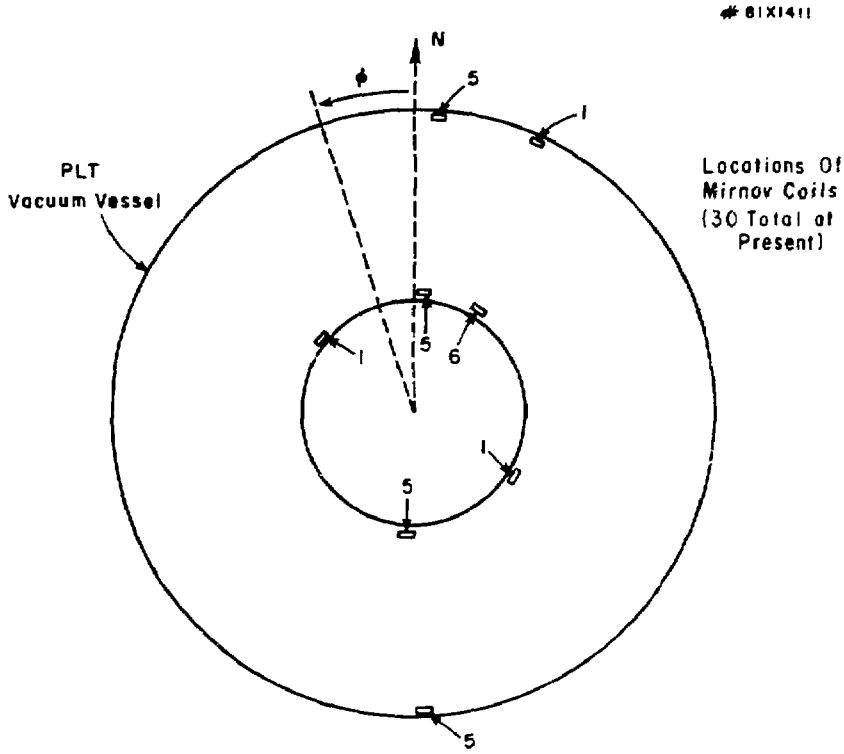

16 Identical Channels

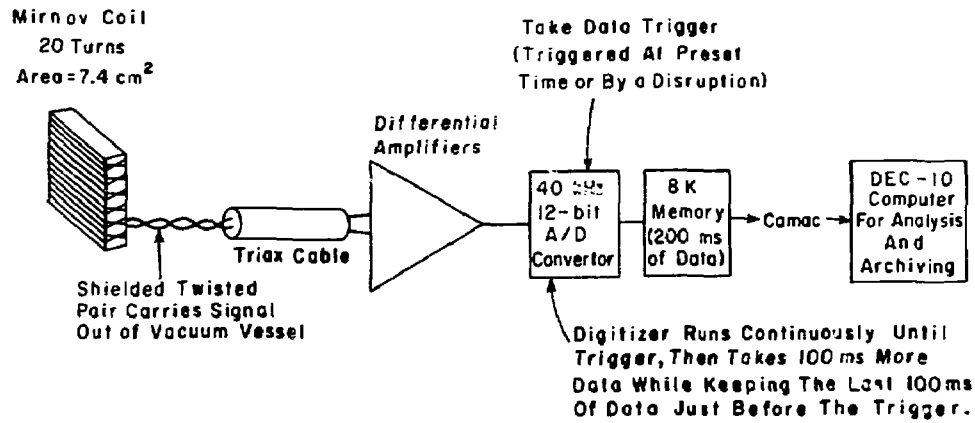

Fig. 6

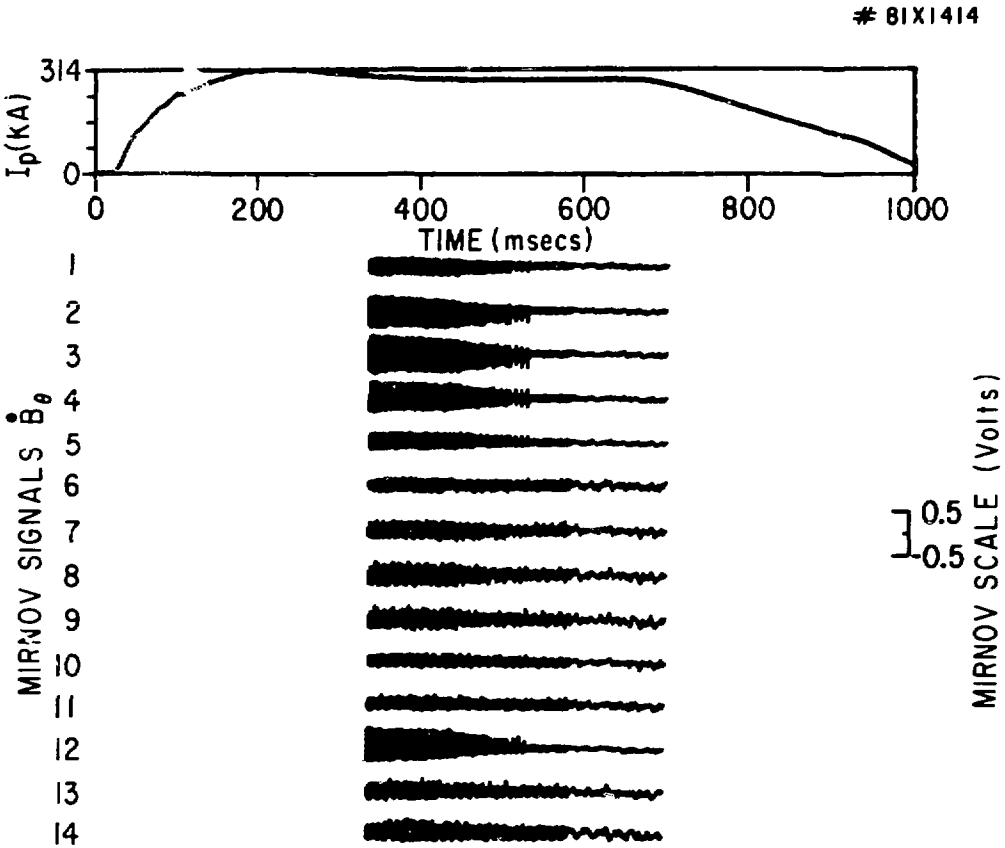
81X1414
314
0
I_p(kA)
0
200
400
600
800
1000
TIME (msecs)
MIRNOV SIGNALS $\dot{B}_\theta$
1
2
3
4
5
6
7
8
9
10
11
12
13
14
0.5
0.5
MIRNOV SCALE (Volts)

Fig. 7

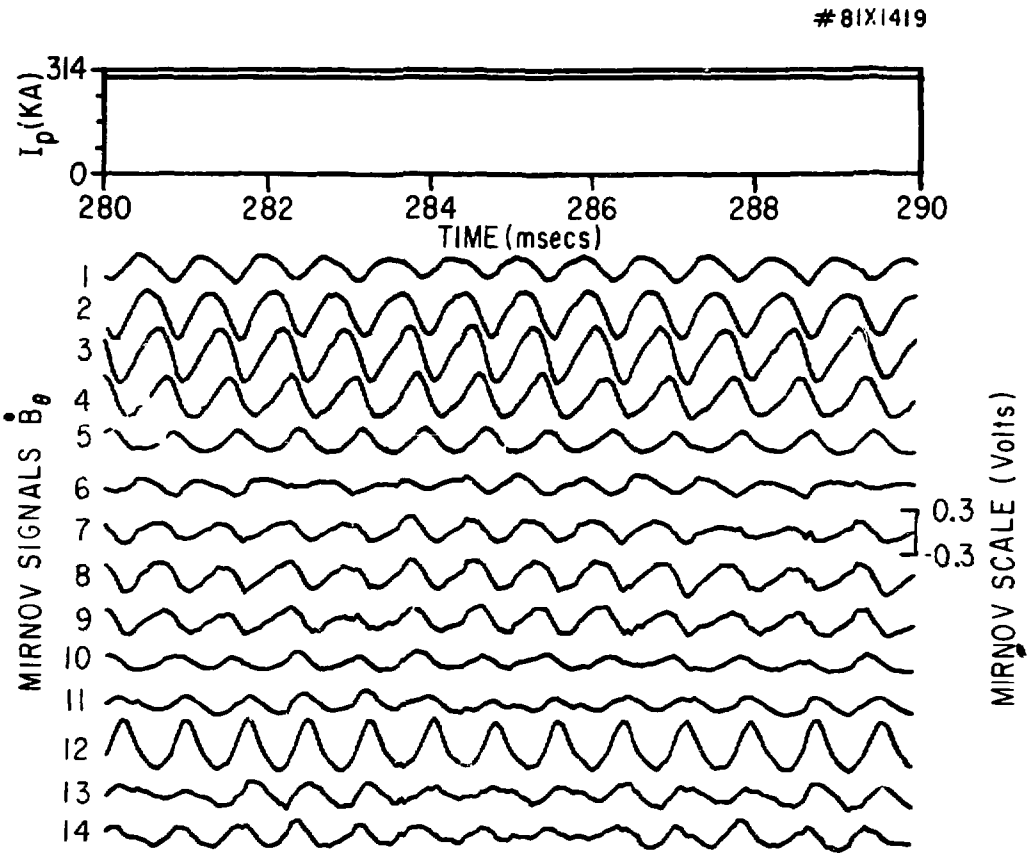
#81X1419
I_p(KA)
314
0
280
282
284
286
288
290
TIME (msecs)
MIRNOV SIGNALS $\dot{B}_\theta$
1
2
3
4
5
6
7
8
9
10
11
12
13
14
0.3
-0.3
MIRNOV SCALE (Volts)

Fig. 8

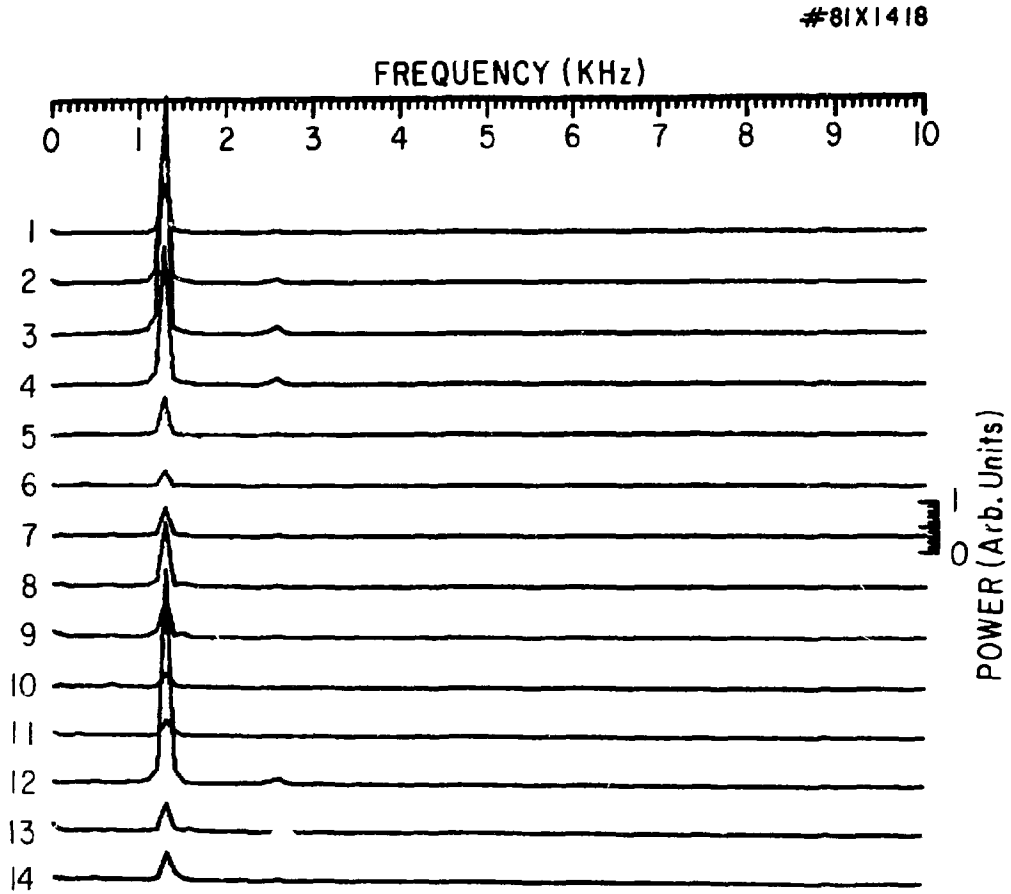
#81X1418
FREQUENCY (KHz)
0
1
2
3
4
5
6
7
8
9
10
1
2
3
4
5
6
7
8
9
10
11
12
13
14
0
POWER (Arb. Units)

Fig. 9

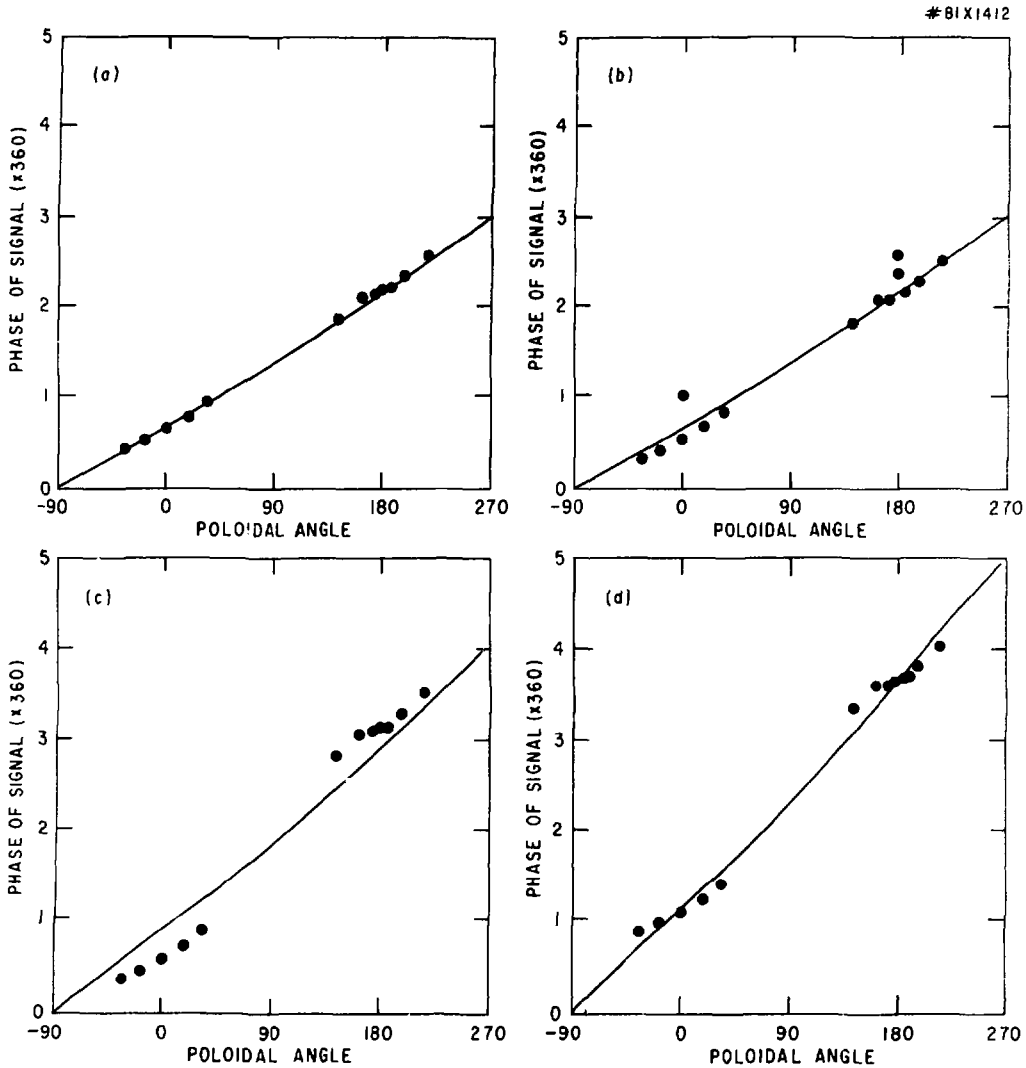
#81X1412
(a)
(b)
(c)
(d)
PHASE OF SIGNAL (x360)
POLOIDAL ANGLE
-90
0
90
180
270
0
1
2
3
4
5

Fig. 10

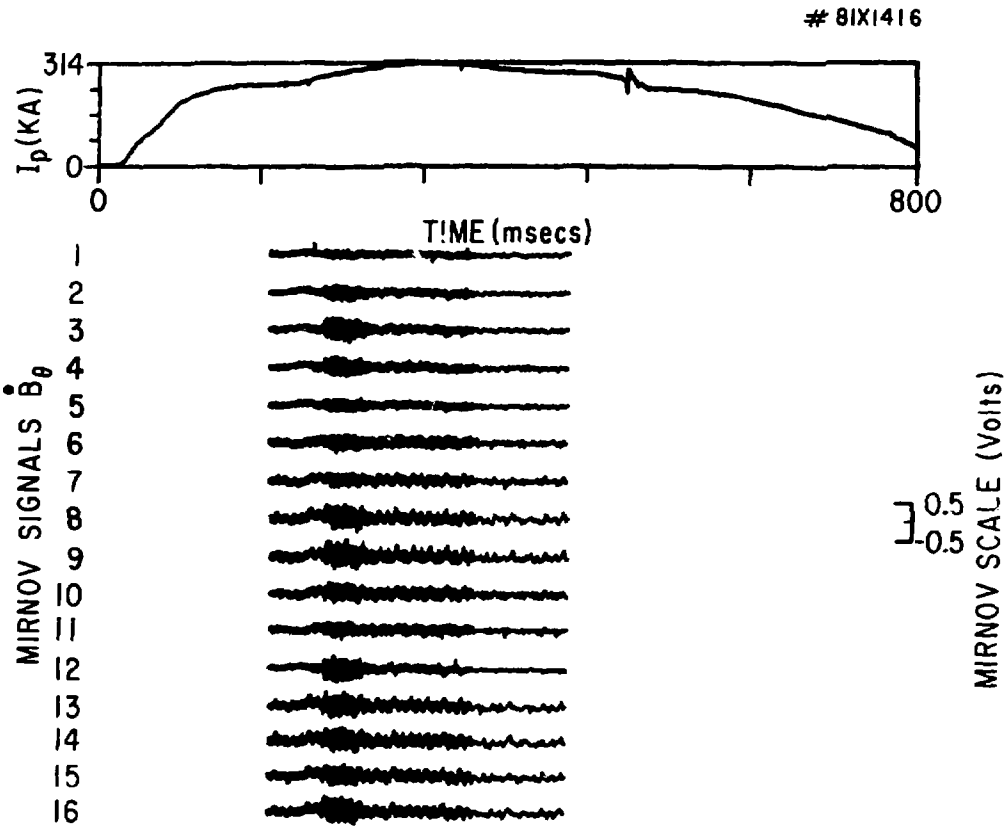
81X1416
314
I_p(KA)
0
0
800
TIME (msecs)
MIRNOV SIGNALS $\dot{B}_\theta$
1
2
3
4
5
6
7
8
9
10
11
12
13
14
15
16
0.5
-0.5
MIRNOV SCALE (Volts)

Fig. 11

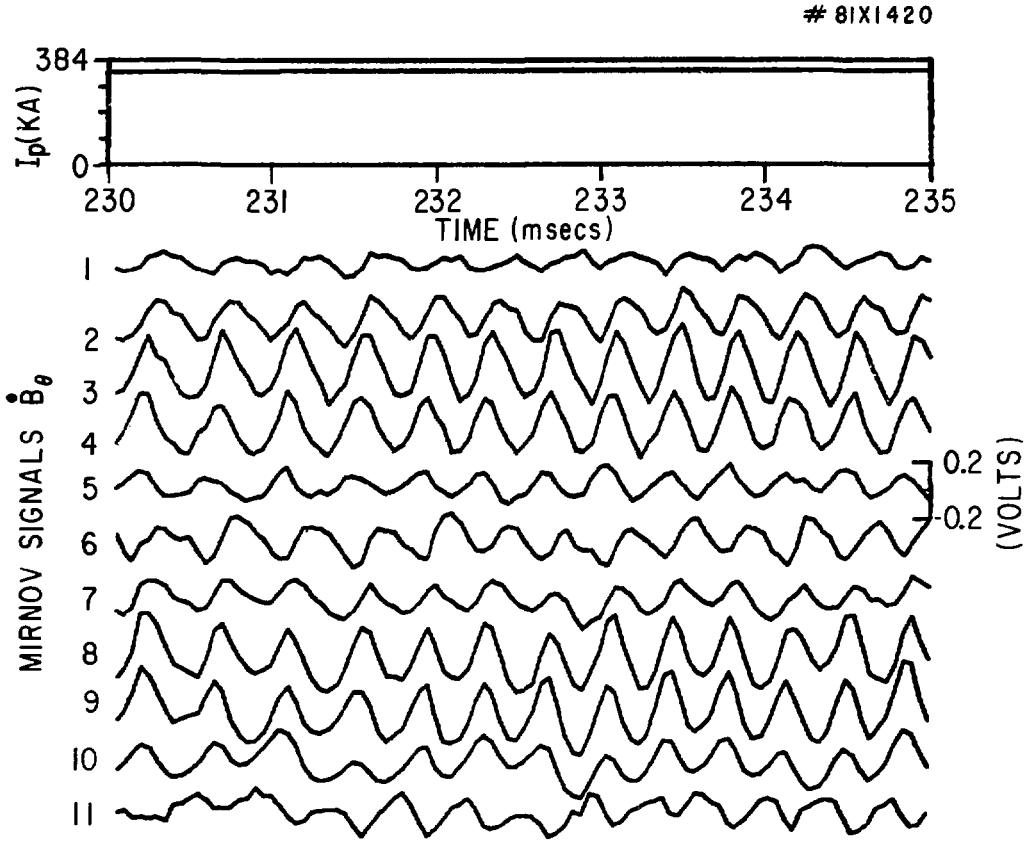
#81X1420
384
0
I_p(KA)
230
231
232
233
234
235
TIME (msecs)
MIRNOV SIGNALS $\dot{B}_\theta$
1
2
3
4
5
6
7
8
9
10
11
0.2
-0.2
(VOLTS)

Fig. 12

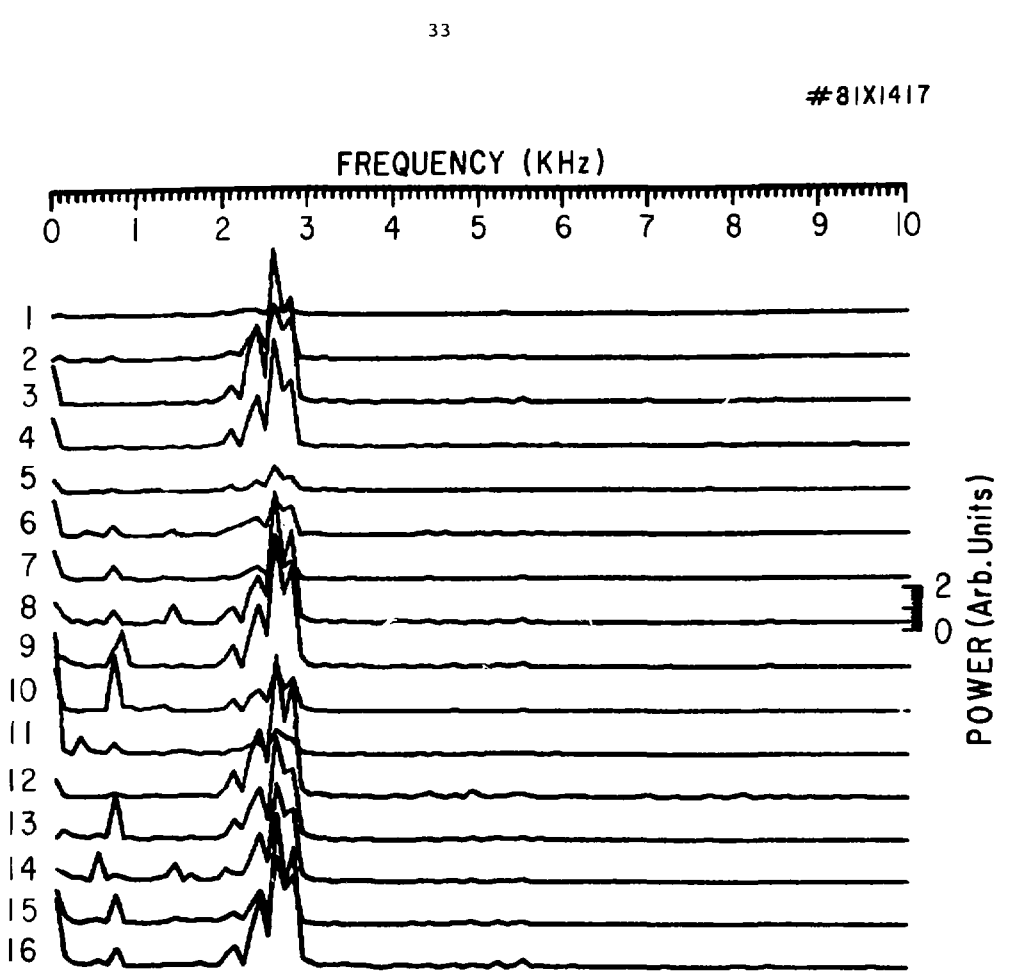
#81X1417
FREQUENCY (KHz)
0
1
2
3
4
5
6
7
8
9
10
1
2
3
4
5
6
7
8
9
10
11
12
13
14
15
16
2
0
POWER (Arb. Units)

Fig. 13

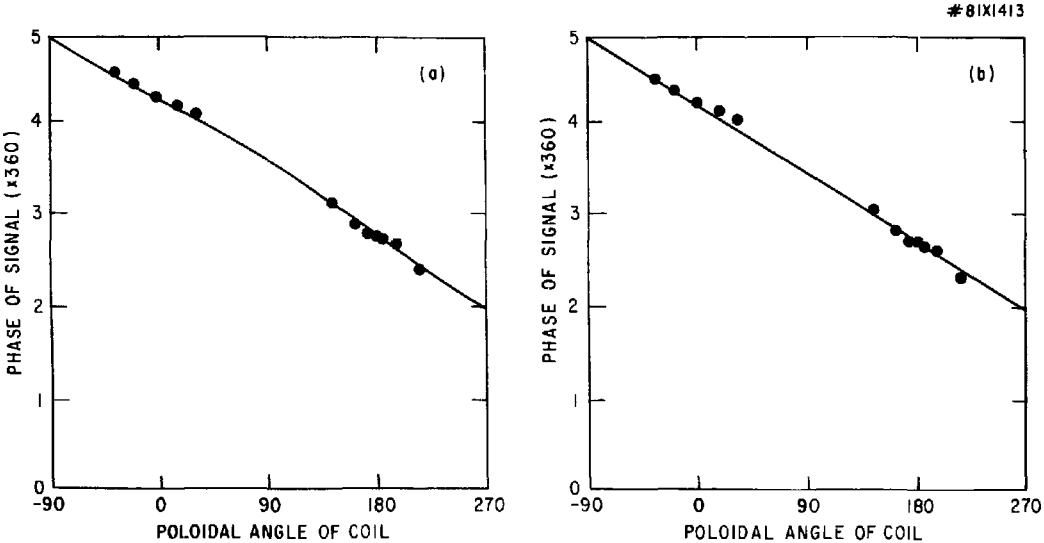
#81X1413
(a)
(b)
PHASE OF SIGNAL (x360)
POLOIDAL ANGLE OF COIL
0
1
2
3
4
5
-90
0
90
180
270

Fig. 14